

High-Mobility Field-Effect Transistors Fabricated with Macroscopic Aligned Semiconducting Polymers

Hsin-Rong Tseng, Hung Phan, Chan Luo, Ming Wang, Louis A. Perez, Shrayesh N. Patel, Lei Ying, Edward J. Kramer, Thuc-Quyen Nguyen,* Guillermo C. Bazan,* and Alan J. Heeger*

Organic field-effect transistors (OFETs) continue to attract interest because of improvements in the charge carrier mobility and lifetime stability. OFETs are promising for use in “plastic electronics” with unique properties including flexibility, transparency, and solution-processibility for high throughput manufacturing methods such as roll-to-roll coating and inkjet printing.^[1–5] Significant progress has been made in solution-processed OFETs based on the use of conjugated small molecules and polymers as the semiconducting material in the FET channel. Charge carrier mobilities (μ) of 10 cm²/Vs achieved recently make such devices useful for industrial application.^[5–7] Semiconducting polymers offer better potential for film forming and mechanical properties, compared with their small molecule counterparts.^[3,8,9] Several strategies including process optimization^[10–14] and molecular design^[9–17] have been proposed to achieve order within the polymer fibers and better polymer packing.

One of the important variables for achieving high charge carrier mobility in OFETs is the polymer molecular weight (MW).^[16,18–20] Low MW materials tend to form crystalline domains, and the “grain boundaries” significantly reduce the carrier mobility.^[21,22] For high-performance high-molecular-weight polymers, the presence of interconnected aggregates is required for high carrier mobility.^[23] From the synthesis point of view, the production yield for high MW materials with low polydispersity remains a challenge. In addition, high MW materials also present difficulties during the fabrication process. They are often difficult to dissolve, and the high viscosity limits utility in high-resolution inkjet printing.

In our previous work high-MW, regioregular poly[4-(4,4-dihexadecyl-4H-cyclopenta[1,2-b:5,4-b']dithiophen-2-yl)-*alt*-[1,2,5]thiadiazolo[3,4-c]pyridine] (PCDTPT, 300 kDa, Scheme 1)

showed higher carrier mobility than lower MW PCDTPT (100 kDa) in OFETs fabricated by drop-casting the semiconducting material.^[24] A method of combining nano-grooved substrates and slow drying in a tunnel-like configuration was demonstrated to align the polymer into highly oriented fibers and thereby achieve chain orientation and order which showed significant gains in the charge mobility. A hole mobility of 6.7 cm²/Vs was demonstrated for high MW PCDTPT.^[24] It would be ideal for widespread practical implementation if one could achieve long-range alignment of low MW polymer semiconductors by a simple method in order to achieve high carrier mobility.

We report here a systematic study of OFETs fabricated with PCDTPT of several MWs (ranging from 30 to 300 kDa) to understand the relationship between MW and carrier mobility. By achieving better orientation and higher fiber density, mobilities as high as 23.7 cm²/Vs have been demonstrated. Interestingly, we find that these high mobility values are relatively insensitive to MW. This is consistent with long-range alignment of the semiconducting polymer chains such that the transport occurs dominantly along the conjugated backbone with occasional π - π hopping to neighboring chains.

Regioregular PCDTPT was synthesized according to previous procedures^[15] and was then separated into different MW fractions (30, 50, 80, 160, and 300 kDa) by gel permeation chromatography (GPC). The MW distributions and PDI are provided in Figure S1 and Table S1 (Supporting Information). Bottom gate, bottom contact field effect transistors were fabricated with the architecture “Si (500 μ m)/SiO₂ (300 nm)/Au (50 nm)/decyltrichlorosilane/PCDTPT” by slow drying in the tunnel-like configuration with a tilt angle \sim 13° on nano-grooved substrates.^[24] For comparison, FETs with the same architecture were made by drop-casting onto normal substrates (without surface grooves).

Figure 1 summarizes the carrier mobilities obtained from the FETs in the saturation regime as a function of MW. In Figure 1A, the average mobilities obtained by drop-casting without polymer chain alignment are 1.9, 1.3, 1.2, 0.7, 0.7 cm²/Vs for 300, 160, 80, 50, and 30 kDa, respectively. These results show a slight MW dependence on mobility, where higher MW gives higher carrier mobility; similar to data reported previously in the literature.^[16,19,20] On the other hand, Figure 1B shows that higher average mobilities that are insensitive to MW can be obtained by using nano-grooved substrates that orient polymer films through self-assembly to fabricate the FETs. We find that polymer orientation is of principal importance to achieve high mobility. As shown in Figure 1B, the mobility for the 50 kDa polymer is $\mu = 23.7$ cm²/Vs, the highest value reported for polymer OFETs (the average value of ten independently

H.-R. Tseng, H. Phan, C. Luo, M. Wang, S. N. Patel,
L. Ying, Prof. E. J. Kramer, Prof. T.-Q. Nguyen,
Prof. G. C. Bazan, Prof. A. J. Heeger
Center for Polymer and Organic Solids
Mitsubishi Chemical Center for Advanced Materials
University of California
Santa Barbara
Santa Barbara, CA 93106, United States
E-mail: quyen@chem.ucsb.edu; bazan@chem.ucsb.edu;
ajhe1@physics.ucsb.edu
L. A. Perez, S. N. Patel, Prof. E. J. Kramer
Materials Department
University of California
Santa Barbara
Santa Barbara, CA 93106, United States



DOI: 10.1002/adma.201305084



Scheme 1. Molecular structure and regioregularity pattern of PCDTPT. The arrows are guides to the eye to highlight stereoregularity.

fabricated FETs is $16.3 \text{ cm}^2/\text{Vs}$). Figure 1C and Figure 1D show the transfer and output curves of the best device.

The transfer curve in Figure 1C shows non-linear behavior, which has been observed in other high mobility system.^[20] We note that the output data at high V_g do not show saturation. Thus, we calculate the mobility using the slope in the low V_g regime ($V_g < 20 \text{ V}$) for which there is good saturation and for which the standard formula is valid. The apparent mobility variation as a function of gate bias is shown in Figure S2.

In order to understand the insensitivity of the mobility to MW, both non-oriented and oriented film morphologies have been characterized by atomic force microscopy (AFM) at the surface and bottom interface. **Figure 2A-B** and Figure S3 (Supporting Information) shows the topography of the films made by drop casting on normal substrates. Nano-scale polymer fiber structures form for all MW fractions. The macroscopic morphology changes dramatically, however, from 300 kDa to low 30 kDa (Figure 2A-B). The polymer fiber structure is directionally random for the high-MW PCDTPT (Figure 2A), whereas the fiber structures become larger and well-defined apparently crystalline domains are observed for low MW polymers (Figure 2B). In each domain, the fibers are aligned parallel to one direction, indicating that the lower MW polymers have better packing and tend to form ordered fibers. As seen in the AFM phase image of the 30 kDa polymer FET film, (Figure S3F), the polymer fibers within a domain are aligned over lengths approaching the micrometer scale. However, there are disordered grain boundary regions between domains. These create trapping sites for charge transport and thereby limit the carrier mobility.^[25] As a result, the carrier mobility decreases as the MW decreases in these non-aligned polymer FETs.

Carrier mobilities for all the MW ranges have been dramatically improved (see Figure 1A-B) due to the formation of well-aligned polymer fibers after slow drying on nano-grooved substrates. Images of both the topside and bottom-side (the side of polymer film contacted to gate insulator) morphology of the PCDTPT layer with MW = 300 and 50 kDa are shown in Figure 2C-F. The polymer fibers are well aligned over long distances for both films, but are slightly different for low MW and high MW materials. Clear fiber structures are seen in the 50 kDa

film (Figure 2D), but more bridging branches are observed between polymer fibers in the 300 kDa film (Figure 2C). These images indicate that shorter chain length polymers are easier to confine and be aligned by the surface grooves. Well-aligned and highly dense fiber formation can be observed from the bottom-side of the films (Figure 2E-F), indicating that the polymer packing is strongly affected by the nano-grooves on the orienting surface. Polymer fibers in the 50 kDa film are well-aligned in one direction, but within the 300 kDa film, some fibers are oriented at slightly different angles. More importantly, the grain boundaries in 50 kDa material disappear after polymer fiber alignment, resulting in high carrier mobility.

The orientation of the films cast on the nano-grooved substrates was further investigated by transmission electron microscopy (TEM) using electron diffraction (ED); the data are presented in Figure S4. With the electron beam orthogonal to the film (0° tilt angle, Figure S4A), the ED pattern consists of very sharp reflections corresponding to the (010) π - π stacking of the crystalline lattice. The angular spread of the (010) reflection in the plane of the film indicates that all the polymer backbone axes of the polymer crystallites are oriented within $\pm 12^\circ$ of the alignment axis. With the sample tilted 70° (Figure S4B), the ED pattern shows exceptional alignment as indicated by the very sharp reflections corresponding to the alkyl side-chain packing (100) of the crystalline lattice. The ED results indicate the aligned polymer chains have an “edge-on” orientation relative

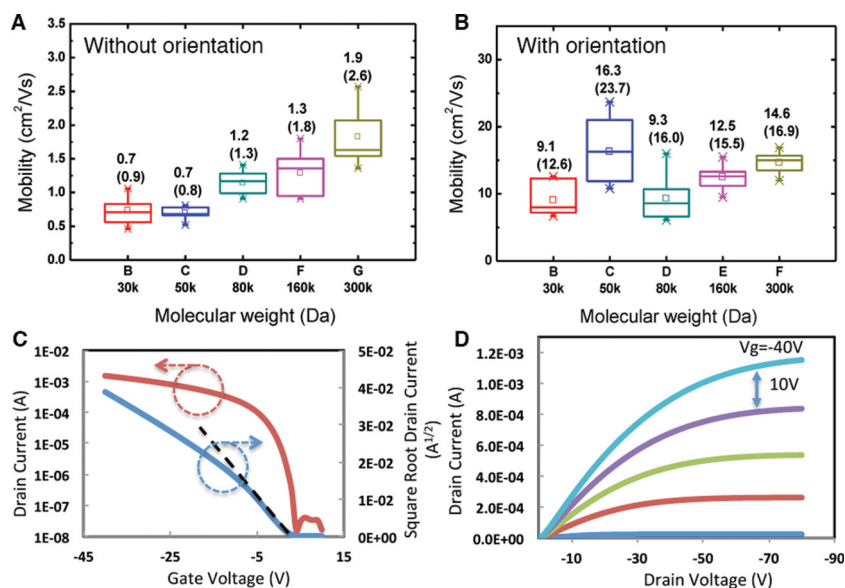


Figure 1. Mobility of PCDTPT OFETs after annealing at 200°C . The mobility value and the value in parentheses represent mean and maximum values obtained from 10 independent OFETs. (A) Devices fabricated by drop casting. (B) Devices fabricated by slow drying in the tunnel-like configuration. The horizontal lines in the box denote the 25th, 50th, and 75th percentile values. The error bars denote the 5th and 95th percentile values. The open square inside the box denotes the mean value. (C) and (D) FET characteristics of PCDTPT with mobility of $23.7 \text{ cm}^2/\text{Vs}$. ($L = 80 \mu\text{m}$, $W = 1 \text{ mm}$): (C) transfer curves taken at $V_{DS} = -80 \text{ V}$ (D) output curves taken at various V_G (0 – 40 V).

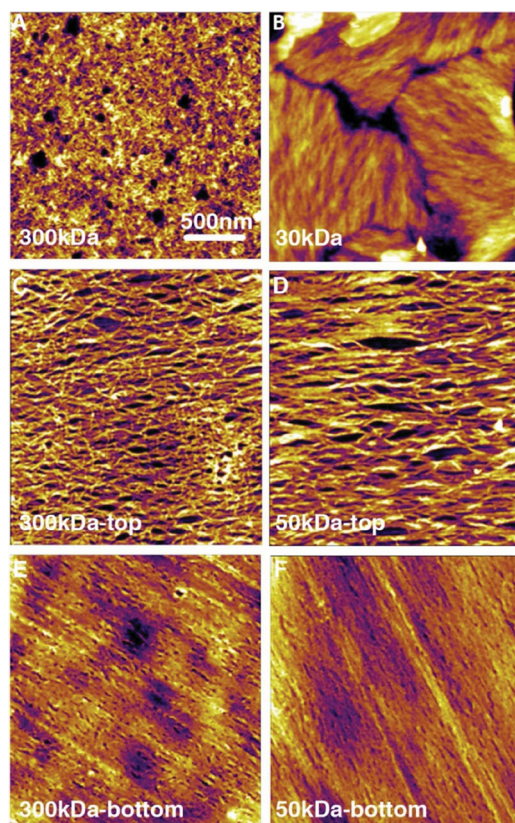


Figure 2. AFM images of the PCDTPT topography by drop-casting on normal polished Si substrates (without orientation): (A) MW = 300 kDa, and (B) MW = 30 kDa. AFM images of PCDTPT topside morphology by slow-drying on nano-grooved substrates (with orientation): (C) MW = 300 kDa and (D) MW = 50 kDa. (E) and (F) show bottom-side morphology with polymer orientation: (E) MW = 300 kDa and (F) MW = 50 kDa.

the scratched substrates. Overall, these results provide further evidence that the alignment of the polymer chains plays a crucial role in enhancing the mobility.

Higher resolution AFM images (250 nm × 250 nm) of the topside morphology of 300 kDa MW film on nano-grooved substrates are shown in **Figure 3**. The individual fibers are clearly aligned within the fiber bundles in the phase image in **Figure 3A**. There is no evidence of any “grain boundaries” in the fiber bundles, which is consistent with the high mobility observed. The width of individual fiber is ~2–3 nm as shown by a cross-sectional AFM line cut surface profile in **Figure 3B**, and is comparable to the length of the repeat unit (~2.4 nm, **Figure 3C**). The only way for polymer chains to align is therefore along the fibers. In addition, the mobility is higher along the fiber and the optical absorption is anisotropic,^[24] consistent with our hypothesis that carriers transport along the conjugated polymer backbone. The dominant intrachain

charge transport in high-mobility semiconducting polymer has also been recently proposed using optical characterization.^[26]

The temperature-dependence of the mobility was investigated for OFETs with MW of 50, 160, and 300 kDa materials aligned on nano-grooved substrates (**Figure 4**). In all the cases, the mobility is thermally activated with an activation energy ~30 meV, as extracted in the temperature range from 85 K to 180 K. The nonlinear behavior of the mobility near and above 200 K could result from the bias stress^[27] or residual moisture in the film.^[28–30] Note that the activation energy is low compared to most other high-mobility polymers,^[31–34] implying that inter-chain carrier hopping is efficient. The low activation energy is consistent with the observation that there are no grain boundaries from chain-to-chain or fiber-to-fiber.^[21]

Grazing incidence wide-angle X-ray diffraction (GIWAXS) was performed to probe the polymer order for the different MW ranges. The data (see **Figure S5** in Supporting Information) are collected by an area detector where azimuthal integrations are performed to produce line cuts. The line cuts for PCDTPT with MW of 30, 50, 80, 160, and 300 kDa are plotted as counts (intensity) versus the scattering vector (q (nm⁻¹)) in **Figure 5A**. The two length scale regimes commonly investigated in conjugated polymer thin films are from $q \sim 1$ –10 nm⁻¹, which corresponds to the lamellar side chain packing and backbone, and the q range of ~12–20 nm⁻¹ describing the π - π stacking between ordered polymer segments.^[35] The positions of the peaks are the same for all the MWs, which means that the MW does not affect the final structure that is formed; however the full width at half-maximum (FWHM) of the alkyl stacking peaks shows a MW dependence. The crystalline correlation length (CCL) of alkyl and π - π stacking were estimated by the Scherrer equation and the data are shown in **Figure 5B**.

The CCL of alkyl stacking changes from 20 nm for 30 kDa to 11 nm for 300 kDa polymer fraction. On the other hand, the CCL of π - π stacking is ~4 nm for all MWs. The independence on the MW of the CCL of π - π stacking, in combination with the MW-independent activation energy shown in **Figure 4**, support the result that carrier transport is predominately along the backbone of the chain with occasional hopping through π - π

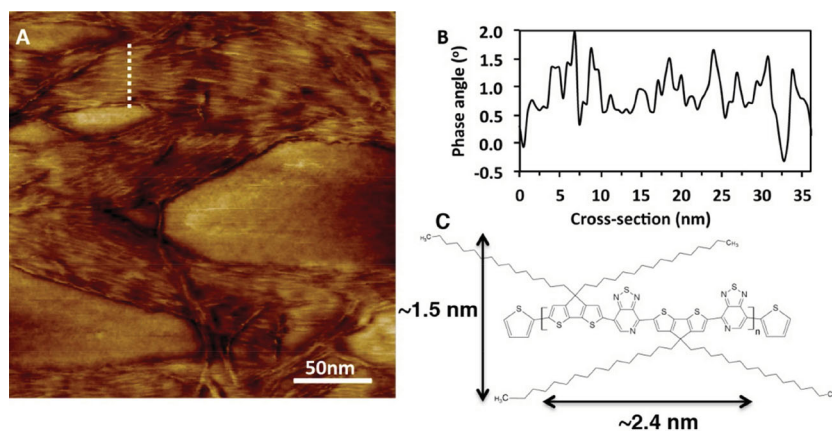


Figure 3. (A) High resolution AFM (250 nm × 250 nm) topside morphology phase image of PCDTPT 300 kDa OFET. (B) The cross-section profile of the dashed line in (A). (C) Molecular structure and estimated size of PCDTPT. The length of one monomer is approximately 2.4 nm and the width (including the side chains) is approximately 1.5 nm.

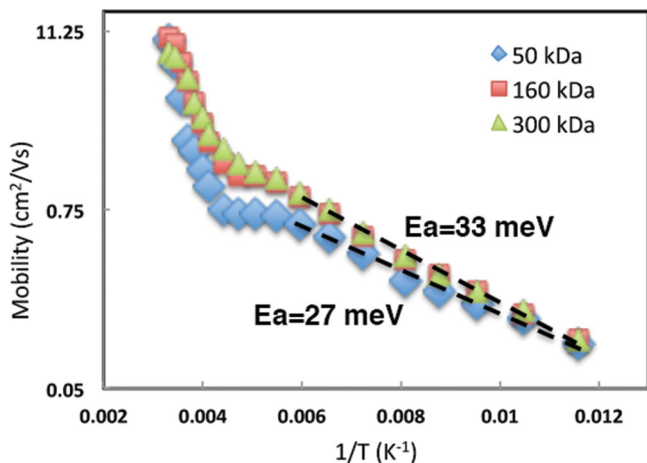


Figure 4. Temperature-dependent mobility for the OFETs with MW of 50, 160, and 300 kDa.

stacking to a neighboring chain, followed again by transport along the backbone. In this way, the mobility is insensitive to MW, and high mobility can be achieved after polymer alignment over long distances.

To summarize, the hole mobility, $\mu = 23.7 \text{ cm}^2/\text{Vs}$, for transport predominantly along the conjugated chain is demonstrated with aligned PCDTPT (MW = 50 kDa). Studies of the MW dependence of the mobility of polymers with long-range alignment obtained by slow drying in the tunnel-like configuration atop nano-grooved substrates indicate that very high MW is not necessary for achieving high mobility. The mobility has been dramatically improved (by about one order of magnitude) and shown to be insensitive to MW after polymer alignment. As a general strategy for continuing improvement of the carrier mobilities, polymer chain fiber alignment facilitates carrier transport along the conjugated polymer backbone with occasional hopping to neighboring chains through π - π stacking.

Experimental Section

PCDTPT Fractionation: The preparative Gel Permeation Chromatography (GPC) instrumentation was equipped with a Waters 1525 binary HPLC pump, an Agilent Technologies PLGEL PREP column (10 μm , 10E5Å, 300×25MM, HMW, part # PL1210–6150) and two detectors (Waters 2414 Differential Refract Meter and Waters 2998 Photodiode Array Detector). The eluent was chloroform with 0.25% (v/v) of triethylamine. The analytical GPC was equipped with a pump (Waters Alliance HPLC System, 2690 Separation Module), two columns (Agilent, PLGEL 5 μm , MIXED-D, 300×7.5 mm) and two detectors (Waters 2410 Differential Refract Meter and Waters 2998 Photodiode Array Detector). The eluent was chloroform with 0.25% (v/v) of triethylamine and at a flow rate of 1 mL/min. The molecular weight was calibrated against polystyrene standards.

The polymer was dissolved in chloroform with 0.25% (v/v) of triethylamine (2 mg/mL). Then the solution was injected into the preparative GPC and eluted at a flow rate of 10 mL/min. The fractions were collected every 10 seconds and their molecular weights were determined by the analytical GPC respectively. Then several fractions were combined according to their molecular weights. The combined solution was concentrated under reduced pressure and precipitated into methanol. The polymer was filtered off and dried under vacuum line.

Device Preparation: The nano-grooved substrates were introduced on the surface of SiO_2 gate dielectric layer by scratching the surface with diamond lapping films (from Allied High Tech Products Inc.) with nanoparticle sizes of 100 nm. A home-made scratching machine is made for this purpose, shown in Figure S6 in SI. Firstly the diamond lapping film is fixed on the stage and the silicon wafer is fixed on a moving holder facing the diamond film. The moving holder then goes down on the wafer to contact the diamond film; the pressure is adjusted to about 0.1 kg/cm². The holder can move forward and backward in one direction for total scratching distance ~1.5 m to induce the parallel grooves on the substrate. During the scratching process deionized water is required between the wafer and diamond lapping film to achieve uniform surface grooves with high density. Source/drain contacts (50 nm thick gold) were then deposited on top of the resulting nano-grooved SiO_2 . Bottom gate, bottom contact field effect transistors with the architecture “Si (500 μm) / SiO_2 (300 nm)/Au (50 nm)/decyltricholosi-lane/copolymer” were fabricated by slow drying in the tunnel-like configuration with a tilt angle 13° on nano-grooved substrates. Additional transistors with same architecture by drop casting on normal substrates (without surface grooves) were made for comparison. The solution concentration is 0.25 mg/mL. The channel length was 80 μm with channel width of 1 mm. Average data were calculated from analysis of 10 independent

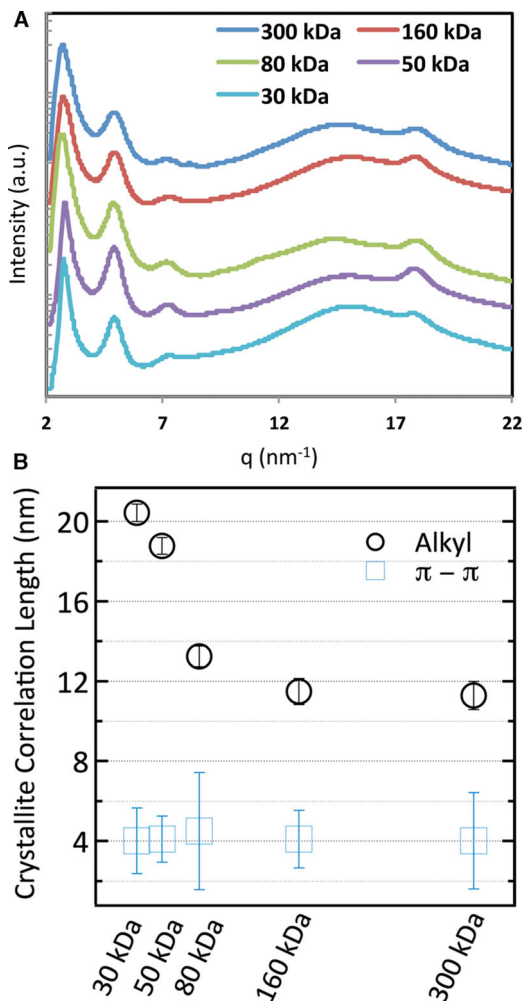


Figure 5. (A) Grazing wide-angle X-ray scattering line profiles of PCDTPT films formed by drop casting. (B) Estimated crystallite correlation length of alkyl and π - π stacking.

devices. Pre-patterned substrates (Si/SiO₂/Au) were first cleaned by ultra-sonication in acetone for 3 minutes and isopropanol 3 minutes, and then dried in an oven (in air) at 120 °C for 10 minutes. The samples were then surface-activated with acid hydrolysis, and dried again in the oven under the same conditions. After treatment by UVO₃ for 15 minutes, the substrates were passivated by decyltricholohsilane from 1 vol.% toluene solution at 80 °C for 25 minutes. After rinsing the substrate with toluene and drying under nitrogen flow, the polymer semiconductors were cast onto the substrate. The samples were annealed at 200 °C for 8 min before measurement. All film deposition, annealing, and current-voltage characterization were done under a nitrogen atmosphere. The capacitances are 10 and 11.5 nF/cm² for normal and nano-grooved substrates.

Device Characterization: Field effect mobilities were obtained in the saturation region of transistor operation by using the equation, $I_{DS} = (W/2L) C_i \mu (V_{GS} - V_{th})^2$, where W/L is the channel width/length, C_i is the gate dielectric layer capacitance per unit area, and V_{GS} and V_{th} are the gate voltage and threshold voltage. The I-V characterization at temperatures from 80 K to 300 K was performed with a Lakeshore vacuum probe-station under a vacuum of $<10^{-6}$ mbar using a Keithley 4200 semiconductor parametric analyzer. The devices were heated at 400 K in vacuum for 7 hours prior to the temperature-dependent measurements. Mobilities were calculated in the saturation regime at $|V_G - V_T| = 15$ V and $V_D = -90$ V for all temperatures. Tapping mode AFM images were obtained using an Asylum MFP-3D Standard System at room temperature to study the topography of the nano-grooved surface and the polymer thin film. High resolution AFM was performed using a Bruker Multimode AFM system under nitrogen atmosphere. Polarized UV-Vis absorption spectra were recorded at room temperature on a PerkinElmer (Lambda 750) spectrophotometer, with the incident light polarized along a certain direction by a broadband thin film polarizer (Melles Griot). The samples for the polarized absorption were prepared on nano-grooved glass substrates with same process used for the device fabrication. Grazing incidence wide angle X-ray scattering (GIWAXS) measurements were performed at beamline 11-3 at the Stanford Synchrotron Radiation Lightsource (SSRL) with an X-ray wavelength of 0.9752 Å, at a 400 mm sample to detector distance. Samples were scanned for 90 s in a He environment at an incident angle of 0.12°. The measurements were calibrated using a LaB6 standard. The crystalline correlation length (CCL) of alkyl and π - π stacking were estimated by the Scherrer equation below:

$$CCL = \frac{2\pi}{FWHM} \quad (1)$$

Supporting Information

Supporting Information is available from the Wiley Online Library or from the author.

Acknowledgements

This research was supported by the MC-CAM Program at UCSB sponsored by Mitsubishi Chemical Corporation (Japan). LAP acknowledges support from the ConvEne IGERT Program (NSF-DGE 0801627) and a Graduate Research Fellowship from the National Science Foundation (GRFP). TQN thanks the Camille Dreyfus Teacher Scholar Award and the Alfred Sloan Research Fellowship program. Portions of this research were carried out at the Stanford Synchrotron Radiation Lightsource user facility operated by Stanford University on behalf of the U.S. Department of Energy, Office of Basic Energy Sciences. This work made use of MRL Central Facilities supported by the MRSEC Program of the National Science Foundation under award No. DMR 1121053. The authors would like to thank Christopher J. Takacs,

Ben B. Y. Hsu, Huiqiong Zhou, Yuan Zhang, Peter Zalar and Martijn Kuik for constructive discussion and technical support.

Received: October 11, 2013

Revised: December 13, 2013

Published online: February 6, 2014

- [1] S. R. Forrest, *Nature* **2004**, *428*, 911–918.
- [2] H. Sirringhaus, N. Tessler, R. H. Friend, *Science* **1998**, *280*, 1741–1744.
- [3] H. Yan, Z. Chen, Y. Zheng, C. Newman, J. R. Quinn, F. Dötz, M. Kastler, A. Facchetti, *Nature* **2009**, *457*, 679–686.
- [4] A. C. Arias, J. D. MacKenzie, I. McCulloch, J. Rivnay, A. Salleo, *Chem. Rev.* **2010**, *110*, 3–24.
- [5] Y. Diao, B. C.-K. Tee, G. Giri, J. Xu, D. H. Kim, H. A. Becerril, R. M. Stoltenberg, T. H. Lee, G. Xue, S. C. B. Mannsfeld, Z. Bao, *Nat. Mater.* **2013**, *12*, 665–671.
- [6] H. Minemawari, T. Yamada, H. Matsui, J. Tsutsumi, S. Haas, R. Chiba, R. Kumai, T. Hasegawa, *Nature* **2011**, *475*, 364–367.
- [7] J. Li, Y. Zhao, H. S. Tan, Y. Guo, C.-A. Di, G. Yu, Y. Liu, M. Lin, S. H. Lim, Y. Zhou, H. Su, B. S. Ong, *Sci. Reports* **2012**, *2*, DOI 10.1038/srep00754.
- [8] I. McCulloch, M. Heeney, C. Bailey, K. Genevicius, I. MacDonald, M. Shkunov, D. Sparrowe, S. Tierney, R. Wagner, W. Zhang, M. L. Chabynyc, R. J. Kline, M. D. McGehee, M. F. Toney, *Nat. Mater.* **2006**, *5*, 328–333.
- [9] H. Chen, Y. Guo, G. Yu, Y. Zhao, J. Zhang, D. Gao, H. Liu, Y. Liu, *Adv. Mater.* **2012**, *24*, 4618–4622.
- [10] H. Sirringhaus, R. J. Wilson, R. H. Friend, M. Inbasekaran, W. Wu, E. P. Woo, M. Grell, D. D. C. Bradley, *Appl. Phys. Lett.* **2000**, *77*, 406–408.
- [11] W. Pisula, A. Menon, M. Stepputat, I. Lieberwirth, U. Kolb, A. Tracz, H. Sirringhaus, T. Pakula, K. Müllen, *Adv. Mater.* **2005**, *17*, 684–689.
- [12] C. M. Duffy, J. W. Andreasen, D. W. Breiby, M. M. Nielsen, M. Ando, T. Minakata, H. Sirringhaus, *Chem. Mater.* **2008**, *20*, 7252–7259.
- [13] D. M. DeLongchamp, R. J. Kline, Y. Jung, D. S. Germack, E. K. Lin, A. J. Moad, L. J. Richter, M. F. Toney, M. Heeney, I. McCulloch, *ACS Nano* **2009**, *3*, 780–787.
- [14] L. Li, P. Gao, K. C. Schuermann, S. Ostendorp, W. Wang, C. Du, Y. Lei, H. Fuchs, L. D. Cola, K. Müllen, L. Chi, *J. Am. Chem. Soc.* **2010**, *132*, 8807–8809.
- [15] L. Ying, B. B. Y. Hsu, H. Zhan, G. C. Welch, P. Zalar, L. A. Perez, E. J. Kramer, T.-Q. Nguyen, A. J. Heeger, W.-Y. Wong, G. C. Bazan, *J. Am. Chem. Soc.* **2011**, *133*, 18538–18541.
- [16] H. N. Tsao, D. M. Cho, I. Park, M. R. Hansen, A. Mavrinskiy, D. Y. Yoon, R. Graf, W. Pisula, H. W. Spiess, K. Müllen, *J. Am. Chem. Soc.* **2011**, *133*, 2605–2612.
- [17] B.-G. Kim, E. J. Jeong, J. W. Chung, S. Seo, B. Koo, J. Kim, *Nat. Mater.* **2013**, *12*, 659–664.
- [18] M. Brinkmann, P. Rannou, *Macromolecules* **2009**, *42*, 1125–1130.
- [19] R. J. Kline, M. D. McGehee, E. N. Kadnikova, J. Liu, J. M. J. Fréchet, M. F. Toney, *Macromolecules* **2005**, *38*, 3312–3319.
- [20] R. J. Kline, M. D. McGehee, E. N. Kadnikova, J. Liu, J. M. J. Fréchet, *Adv. Mater.* **2003**, *15*, 1519–1522.
- [21] L. H. Jimison, M. F. Toney, I. McCulloch, M. Heeney, A. Salleo, *Adv. Mater.* **2009**, *21*, 1568–1572.
- [22] J. Rivnay, L. H. Jimison, J. E. Northrup, M. F. Toney, R. Noriega, S. Lu, T. J. Marks, A. Facchetti, A. Salleo, *Nat. Mater.* **2009**, *8*, 952–958.

- [23] R. Noriega, J. Rivnay, K. Vandewal, F. P. V. Koch, N. Stingelin, P. Smith, M. F. Toney, A. Salleo, *Nat. Mater.* **2013**, advance online publication, DOI 10.1038/nmat3722.
- [24] H.-R. Tseng, L. Ying, B. B. Y. Hsu, L. A. Perez, C. J. Takacs, G. C. Bazan, A. J. Heeger, *Nano Lett.* **2012**, *12*, 6353–6357.
- [25] H. N. Tsao, K. Müllen, *Chem. Soc. Rev.* **2010**, *39*, 2372–2386.
- [26] X. Zhang, H. Bronstein, A. J. Kronemeijer, J. Smith, Y. Kim, R. J. Kline, L. J. Richter, T. D. Anthopoulos, H. Sirringhaus, K. Song, M. Heeney, W. Zhang, I. McCulloch, D. M. DeLongchamp, *Nat. Commun.* **2013**, *4*, DOI 10.1038/ncomms3238.
- [27] A. Salleo, T. W. Chen, A. R. Völkel, Y. Wu, P. Liu, B. S. Ong, R. A. Street, *Phys. Rev. B* **2004**, *70*, 115311.
- [28] R. A. Street, J. E. Northrup, A. Salleo, *Phys. Rev. B* **2005**, *71*, 165202.
- [29] L. Mattias Andersson, W. Osikowicz, F. L. E. Jakobsson, M. Berggren, L. Lindgren, M. R. Andersson, O. Inganäs, *Org. Electron.* **2008**, *9*, 569–574.
- [30] H. L. Gomes, P. Stallinga, M. Cölle, D. M. de Leeuw, F. Biscarini, *Appl. Phys. Lett.* **2006**, *88*, 082101–082101–3.
- [31] B. H. Hamadani, D. Natelson, *Appl. Phys. Lett.* **2004**, *84*, 443–445.
- [32] J. A. Letizia, J. Rivnay, A. Facchetti, M. A. Ratner, T. J. Marks, *Adv. Funct. Mater.* **2010**, *20*, 50–58.
- [33] M. J. Lee, D. Gupta, N. Zhao, M. Heeney, I. McCulloch, H. Sirringhaus, *Adv. Funct. Mater.* **2011**, *21*, 932–940.
- [34] T.-J. Ha, P. Sonar, A. Dodabalapur, *Phys. Chem. Chem. Phys.* **2013**, *15*, 9735–9741.
- [35] M. L. Chabinyc, *Polym. Rev.* **2008**, *48*, 463–492.